Conductance of amyloid β based peptide filaments: structure–function relations.

Article

Accepted Version

It is advisable to refer to the publisher's version if you intend to cite from the work. See Guidance on citing.

To link to this article DOI: http://dx.doi.org/10.1039/C2SM26017D

Publisher: Royal Society of Chemistry

www.reading.ac.uk/centaur

CentAUR

Central Archive at the University of Reading

Conductance of Amyloid β Based Peptide Filaments: Structure-Function Relations

Moran Amit[1], **Ian W. Hamley**[2], **Nurit Ashkenasy**[1,3]

[1] Department of Materials Engineering, Ben Gurion University of the Negev, Beer-Sheva, Israel

[2] School of Chemistry, University of Reading, Reading, UK

[3] The Ilse Katz Institute for Nanoscale Science and Technology, Ben Gurion University of the Negev, Beer-Sheva, Israel

Abstract

Controlling the morphology of self-assembled peptide nanostructures, particularly those based on amyloid peptides, have been the focus of intense research. In order to exploit these structures in electronic applications, further understanding of their electronic behavior is required. In this work, the role of peptide morphology in determining electronic conduction along self-assembled peptide nanofilament networks is demonstrated. The peptides used in this work were based on the sequence AAKLVFF, which is an extension of a core sequence from the amyloid β peptide. We show that the incorporation of a non-natural amino acid, 2-thienylalanine, instead of phenylalanine improves the obtained conductance with respect to that obtained for a similar structure based on the native sequence, which was not the case for the incorporation of 3-thienylalanine. Furthermore, we demonstrate that the morphology of the self-assembled structures, which can be controlled by the solvent used in the assembly process, strongly affects the conductance, with larger conduction obtained for a morphology of long, straight filaments. Our results demonstrate that, similar to natural systems, the assembly and folding of peptides is of great importance for optimizing their function as components of electronic devices. Hence, sequence design and assembly conditions can be used to control the performance of peptide based structures in such electronic applications.

1   Introduction

The natural ability of peptides and proteins to self-assemble into elongated solid fibrils is associated with neurodegenerative diseases, such as Alzheimer's, Parkinson's, and type II

diabetes.[1, 2] Extensive studies have focused on understanding the self-assembly process of isolated peptides based on protein sequences that are related to those diseases, and its dependence on the sequence and the surrounding media.[3-8] A commonly used sequence is the core sequence of the amyloid β (Aβ) peptide, KLVFF, which is associated with the in Alzheimer's disease. In particular, diphenylalanine was found to be the smallest structural motif from the amyloid β peptide that self-assembles into discrete and stiff nanotubes.[9] Moreover, Hamley and co-workers have demonstrated that the self-assembled structure depends on the polarity of the solvent in which the peptide is suspended. In particular, it was shown that 1 wt %AAKLVFF (an extended form of the Aβ(16-20) peptide, in which two nonaromatic alanine residues have been added to the N-terminus of the peptide) in methanol forms nanotubes,[3, 10] while in water it self-assembles into fibrils.[3, 11]

These self-assembled peptide filaments display diverse properties that makes their use in nanotechnological applications attractive.[12-18] For example, extensive studies of the diphenylalanine nanotubes indicated that they exhibit significant rigidity, mechanical, and thermal stability.[19-22] Furthermore, these nanotubes have shown to possess intrinsic photoluminescence[23-25] and piezoelectric functionality,[26] and their utilization for biosensing and light harvesting has been recently demonstrated.[27-29] The formation of elongated structures with highly hierarchical order - introduce by the self-assembly process − makes these structures appealing for electronic applications.[17, 30] Therefore, several studies investigating the electronic conductance of peptides have been performed. Del Mercato *et al*. characterized the electrical conduction of poly(VGGLG) nanofibrils films in the 30-70% relative humidity range, showing currents in the range of nA,[31] while Castillo *et al*. studied the electrical properties of a single amyloid peptide nanotube that exhibit currents in the pA range.[32] Investigation of the conductivity of peptide nanotube networks was also carried out using impedance spectroscopy measurements.[33] De la Rica *et al*. used this characterization method as well, in order to characterize peptide nanotubes and further implement them into sensor chips for high sensitivity, label-free electrical detection of pathogens.[29] In order to increase the conductivity of peptide nanotubes, the incorporation of non-natural amino acids was suggested.[8, 34-37] Moreover, controlling the self-assembly was used to align the nanotubes vertically with respect to the surface,[38-41] in configurations that can be useful for device fabrication. Using such an architecture, we have recently demonstrated that D,L-α cyclic

peptide self-assembled nanotubes exhibit very efficient charge transport.[41] While these studies, as well as investigations of conduction through proteins,[42-44] indeed imply that their incorporation in electronic devices may become a powerful strategy for the formation of bioelectronic devices, understanding the intrinsic conduction mechanisms and how they are influenced by structural parameters is still required. In this work we demonstrate the dependence of the conductance of networks of self-assembled peptide filaments on the morphology, which is controlled by the peptide sequence as well as the solvent used in the assembly process.

1   Experimental

1.1   Peptide synthesis

Amyloid β –derived peptide were synthesized by standard Fmoc solid phase synthesis methods and were studied as TFA salts. The synthesis of (2-Thi)(2-Thi)VLKAA is described elsewhere,[8] and (3-Thi)(3-Thi)VLKAA was prepared similarly. AAKLVFF was purchased from CS Bio (Menlo Park, CA), with purity above 97%.[3] The purity of the peptides was verified by HPLC.

1.2   Substrate preparation

For conductance measurements, devices consisting of a main electrode, surrounded by seven secondary electrodes, 300 μm wide and with a gap of 20 μm were fabricated on a silicon wafer with a 100 nm thick thermal oxide top layer. All electrodes consisted of 1 μm thick Au layer deposited on 15 nm Ti adhesion layer. This configuration enabled the measurement of up to seven different devices in each experiment. Prior to peptide film deposition, devices, as well as silicon samples with native oxide layer used for scanning electron microscopy (SEM) imaging, were cleaned using freshly prepared Piranha solution (solution of 3:7 30% H_2O_2 and concentrated H_2SO_4) for 20-30 minutes (*Caution: Piranha is a very strong oxidant and reacts violently with many organic materials*), followed by three times washing in triply-distilled water (TDW) (18.2 MΩ, EASYpure®RoDi -Thermo Scientific, USA), and drying under nitrogen flow.

1.3 Peptide assembly

0.03%wt solutions of each of the three peptides were prepared by dissolving the peptides in either TDW or MeOH (HPLC grade A, Sigma Aldrich). In addition, solutions of 1 wt% AAKLVFF in TDW or MeOH were prepared. 5 or 10 µl of each fresh solution was applied on either a chip or a silicon wafer with native oxide layer, and left overnight to dry.

1.4 Morphological characterization

Topography images were acquired by atomic force microscopy (AFM, Solver-Pro, NT-MDT, Russia) in tapping mode using non-contact tips with spring constant of 1.74 N/m and resonant frequency of 90 kHz, (NSG03 NT-MDT, Russia) or 3 N/m and 75 kHz (Multi75Al-G, BudgetSensors, Bulgaria). Cross section measurements and image processing, which included second order polynomial line fitting, were carried out by the NOVA AFM software. SEM imaging was performed using a high resolution SEM (HRSEM JEOL JSM-7400F, Japan) for samples prepared on a silicon wafer.

1.5 Electrical characterization

Current-voltage measurements were acquired in a two electrodes configuration using a probe station (JANIS, U.S.A) connected to a Keithley 2635 Source-Meter instrument. At least ten successful measurements were conducted for each peptide network using at least two different chips. These measurements were conducted under a pressure of 10^{-3} mbar, and were acquired from 0 V to ±2 V in order to avoid large capacitance effects induced by large voltage changes at the beginning of the measurement, using 0.05 V steps and 1 sec sweep delay. Current -voltage (I-V) relations were obtained by averaging the measurements and the error was calculated as the standard deviation of the data. Since the behavior of the curves appeared to be linear in all of the experiments, conductance values were extracted from the slope of the linear-fitted curves, using OriginPro software, and the error of the conductance values was calculated as ~4%.

2 Results and discussion

In order to study the relations between filament structure and electronic conduction we have used the well-studied AAKLVFF peptide sequence (Figure 1a), the self-assembly of which depends on solvent used.[3] In order to further elucidate the role of structural motifs in controlling electronic conduction, two modifications of the peptide were used, in which the two phenylalanine residues were replaced with the non-natural amino acids 2-thienylalanine (2-Thi) and 3-thienylalanine (3-Thi), resulting in the sequences (2-Thi)(2-Thi)VLKAA and (3-Thi)(3-Thi)VLKAA, respectively (Figures 1b and c, respectively). It was postulated that the use of thiophene residues that are widely used for the formation of conducting polymers[45-47] may improve the conductance of the self-assembled peptide structures,[8, 37, 48] while maintaining the self-assembly propensity due to their chemical similarity. Indeed, the morphology of (2-Thi)(2-Thi)VLKAA has been studied thoroughly in different self-assembly conditions.[8] Since both assembly and conductance were expected to depend on the π-π stacking interactions, they were promoted by increasing the distance between the thiophene groups and the negatively charged C-terminus of each peptide. This was obtained by reversing the sequence, *i.e.*, the order of the sequence between the N and C termini was switched.

Electrical measurements were obtained on films of the peptide filaments prepared by the drop-dry method using either TDW or methanol as solvents. This procedure has ensured an equal amount of material deposited for each film, hence enabling comparison of the conductance between the different structures. I-V measurements were conducted under a pressure of 10^{-3} mbar in order to minimize humidity effects. Indeed it was found that conductance values under pressure of 10^{-3} mbar and in 16% relative humidity are rather similar (e.g. for 0.03%wt (2-Thi)(2-Thi)VLKAA assembled in MeOH the conductance values are 2 and 2.5 pS, respectively). High reproducibility was obtained for I-V experiments conducted on different electrodes of the same chip (Figure S1). Moreover, sample to sample reproducibility was found to be high, confirming that the conductance is an inherent property of the networks and can be used to compare between the different peptide networks (Figure S1). No degradation of the conductance was detected after two months of storage, showing high stability of the peptide networks, which is of great importance for future applications. As

a reference, I-V curves were measured on a chip after piranha treatment without peptide deposition.

To study the effect of self-assembly on the conductance, samples prepared from 1 wt% AAKLVFF assembled in MeOH and TDW, were characterized. A network of straight, elongated nanotubes, 20±10 nm in diameter and several microns long, were observed in AFM height and phase images of samples prepared in MeOH (Figure 2a and b, respectively). This is in agreement with previous reports,[3, 10] which suggest the formation of nanotubes under such conditions. We note that the large error in the estimation of the diameter of the nanotubes is due to difficulty in accurate measurement of the height in the AFM image because of large amount of material on the surface. In contrary, 1 wt% peptide assembled in TDW exhibited a morphology of small aggregates that covered the entire surface. A few fibrils were also observed on the surface, the length of which was several micrometers, and their height was 55±15 nm (Figure 2c and d). Twisting of the fibrils could be observed, especially in the phase image, with a pitch of about 0.2 μm (Figure 2 d). I-V curves revealed larger currents for peptide assembled in MeOH then in TDW (Figure 2e). The conductance of the sample prepared from peptide assembled in MeOH was found to be 9 pS, while samples of the same peptide assembled from TDW with the same concentration had much lower conductance (G<0.05 pS). Given that the chemical structure of the peptide is the same, it can be concluded that the difference in conductance is due to the different morphology. This is probably due to the higher self-assembly propensity of the AAKLVFF peptide in MeOH, which results in a larger fraction of ordered nanotubes. As a result a larger number of conduction routes are available. Furthermore, it can be assumed that the intrinsic conductivity of these long nanotubes is better than for the small aggregates due to long range order induced by the self-assembly. These results clearly demonstrate the importance of self-assembly in promoting charge transport across peptide nanostructures. Since self-assembly is controlled by the solvent used for the process, the solvent may play a critical role in determining the electronic properties of peptide based devices.

The effect of peptide side chains was tested by comparing the conductance of the basic amyloid β peptide extended core with peptide analogs in which the phenylalanine residues were replaced by thienylalanine ones. All three peptides were assembled in either TDW or

MeOH with peptide concentration of 0.03 wt%. As can be seen in Figure 3, in most of the cases conductance smaller than 0.05 pS (the experimental sensitivity limit) was observed, comparable to the conductance obtained for a reference sample on which no peptide was deposited. An important exception to this behavior was the non-negligible conductance of 2 pS observed for samples of (2-Thi)(2-Thi)VLKAA prepared in MeOH solution.

Once again, the conductance of peptide assembled from MeOH solution was found to be larger than for the same peptide assembled from aqueous solution. AFM height image of (2-Thi)(2-Thi)VLKAA assembled in MeOH reveals a mesh of fine fibrous material that was composed of two populations, both with typical length of several micrometers but withr diameter varying between 13±5 nm or 45±10 nm (Figure 4a, and corresponding cross-sections in Figure S2a). The same net fibrous structure can be seen clearly in SEM as well (Figure 4b). For the peptide assembled in TDW, AFM height image revealed that the entire surface was covered by a layer of short fibrous material (Figure 4c). The length of these fibers was found to be ~0.5 μm, and the roughness was found to be around 1 nm. In addition, some bundled fibers were observed in the AFM image and in SEM image (Figure 4d). Using a lower magnification AFM image the length of the bundles was found to be ~1 μm with an average diameter of 6±1.5 nm, (Figure S2b and the corresponding cross-section). For this self-assembled peptide morphology no conductance was observed under a pressure of 10^{-3} mbar (Figure 3). Despite the fact that most of the material underwent self-assembly, the obtained conductance was smaller than for the same peptide when assembled into elongated fibers in MeOH. This can be attributed to large inter-fiber resistivity. Hence, the length of the segments in the network, and possibly the magnitude of their persistent length, is shown to be important for conductance characteristics. We note that in previous work,[8] it was shown that this peptide self-assembles into twisted fibrils in both methanol and water solutions. The different assembly conditions may impose different side chain orientation, which could affect the conductance.

The conductance of (2-Thi)(2-Thi)VLKAA assembled in MeOH appears to be smaller than the conductance obtained for AAKLVFF assembled in MeOH, which were presented above (Figure 2). However is should be noted that the peptide concentration of 1 wt% used in the first case for AAKLVFF is almost 2 order of magnitude larger than the amount used in the

second case (0.03 wt%), while the conductance is less than five times greater. In fact, the conductance of AAKLVFF assembled in MeOH at 0.03 wt% was found to be significantly smaller than that of (2-Thi)(2-Thi)VLKAA assembled in MeOH. AFM height image of 0.03 wt AAKLVFF% assembled in MeOH revealed a mixed morphology of a fine net of fibres and wide tapes (Figure 5 a and b). The wide tapes were found to be ~1 μm wide, and had an average height of 10±3 nm, as estimated from large scale AFM images (Figure S2c). The tapes are ascribed to unwrapped nanotube sheets. The diameter of the fibers was found to be 30±13 nm (see corresponding cross-section in Figure S2 c) and their length was in the order of few micrometers, same as the length obtained for filaments of AAKLVFF assembled in MeOH at a peptide concentration of 1 wt%. Since a similar morphology of net of fibrous material of similar dimensions was obtained for both (2-Thi)(2-Thi)VLKAA and AAKLVFF assembled in MeOH at 0.03 wt%, it can be deduced that the increased conductance for the first peptide is due to the replacement of phenylalanine by a thienylalanine amino acid. However, it is not clear whether the chemical identity of the side chain directly affects the conductivity, or whether these changes are due to differences in the self-assembled structure, or the arrangement of the side chains. Furthermore, the conductance could be largely affected by the tape morphology, which might be much lower than for the fibers. A low conductance layer, if separating the fibers and the electrodes, might form an insulating barrier and drastically limit the conductance. Overall, the results clearly demonstrate that chemical changes of the peptide side chains affect the conductance.

Since the conductance of AAKLVFF assembled both in MeOH and TDW at concentration of 0.03 wt% was below the measurement sensitivity limit, differences between the conductance of both samples could not be revealed. However, similar to the higher concentration assemblies, the morphology of the assembled peptide was substantially different in TDW than in MeOH. A layer of fibrous material arranged in grains with size of ~0.4x0.4 μm^2 and height of 3±1 nm, differing in the fibre orientation, was clearly observed in the AFM height image (Figure 5c). In addition, relatively large branched fibrous structures, tens of micrometers long with height of 120±20 nm were obtained, as seen in the SEM image (Figure 5d. See also AFM height image in Figure S2 d and the corresponding cross-section). This morphology does not resemble that for 1 wt% AAKLVFF assembled in TDW, showing the role of peptide concentration in determining the self-assembled morphology as well.

Further insight into the effect of peptide side chains on the conductance was obtained by comparing the conductance for peptide analogs with the different thienylalanine isomer; 3-Thi. A decreased conductance was found for the peptide containing 3-Thi assembled in MeOH (Figure 3). In addition to the decrease in conductance, apparent differences in the morphology were observed (Figures 6a and b). Similar to the assembly of 0.03 wt% AAKLVFF in water, assembly of 0.03%wt (3-Thi)(3-Thi)VLKAA in MeOH resulted in the formation of large tapes, a few micrometers wide with height of ~150 nm (see also Figure S2e for a large scale AFM image). Some of these tapes appeared to be folded or twisted, and in some cases the formation of fibers was observed (marked with green, purple, and blue arrows in Figure S2e). Short fibrous assemblies, with height of 70±25 nm (corresponding cross-sections are presented in Figure S2e) and length varying between 0.5-1 μm, were also observed on the surface in both the AFM and SEM images. The roughness of the surface increased to 2 nm RMS, indicating nonspecific aggregation as well. These morphological differences may explain the differences observed in the conductance. However, we cannot exclude entirely the possibility that altering the side chains also directly affects the conductance, and not just indirectly by imposing different structure.

Assembly of (3-Thi)(3-Thi)VLKAA in TDW resulted in the formation of fibers with typical diameter of 23±5 nm (Figure 6c and corresponding cross-section in Figure S2f). This morphology, which could not be resolved by SEM imaging (Figure 6d), was found to be rather similar to the fine fibrous morphology of (2-Thi)(2-Thi)VLKAA assembled in MeOH, yet the conductance was smaller than 0.05 pS, smaller than the conductance of (2-Thi)(2-Thi)VLKAA assembled in MeOH (Figure 2). While these differences may, in this case, arise due to better conductivity of the 2-Thi side chains, it is important to note that (3-Thi)(3-Thi)VLKAA fibers appeared to be more curved, suggesting shorter persistence length, a morphology that may hinder the conductance. Hence, the differences in the conductance could arise due to longer range order of (2-Thi)(2-Thi)VLKAA assembled in MeOH. It should further be noted that differences in the fine structure of the assemblies, which cannot be resolved by AFM and SEM could greatly affect the conductivity.

As a final test to the importance of peptide side chain in determining the conductance, we have used a peptide with the sequence A_6K. This peptide, which has the same number of

amino acids, has a completely different sequence based on a surfactant-like peptide design with a lengthy hexa-alanine "tail" and charged lysine "headgroup". In particular, this peptide does not contain any aromatic side chain, eliminating the possibility of electron transfer through aromatic π stacks. This peptide adopts a nanotube morphology upon assembly at 15 wt% in aqueous solutions (Figure 7a and b, AFM height and phase images, respectively).[49, 50] Despite the formation of a net of nanotubes with diameters of ~2 nm, and the large amount of peptide deposited on the surface of the device, no conductance was detected within the measurement sensitivity under the same measurements conditions mentioned before (Figure 7c). Since the morphology of the peptide nanostructures is similar to the morphology obtained for 0.03%wt (2-Thi)(2-Thi)VLKAA assembled in MeOH, it appears that the differences in the conductance could be related to the peptide side chains.

3   Conclusions

This work demonstrates the importance of morphology and sequence of self-assembled peptide nanostructures in determining the conductance of networks based on them. Differences in the morphologies of peptides based on amyloid β peptide core sequence were obtained by altering the solvent in which the self-assembly was conducted and/ or by changing phenylalanine residues to thienylalanine ones. The results indicate that the formation of long and stiff nanotubes promotes the conductance. It was shown that the side groups of the peptides affect the conductance. In particular, we confirmed that the conductance was improved upon incorporation of non-natural 2-thienylalanine in the sequence. These changes were mostly attributed to changes induced to the morphology of the assemblies. However, it was shown that for similar structures, but with completely different sequences that do not contain aromatic side chains, lower conductance is obtained. These results indicate that by a proper design of peptide side chains and control of assembly conditions these peptide based nanostructures may become useful components of electronic devices. Nonetheless, further studies are required in order to further increase the conductance of such assemblies.
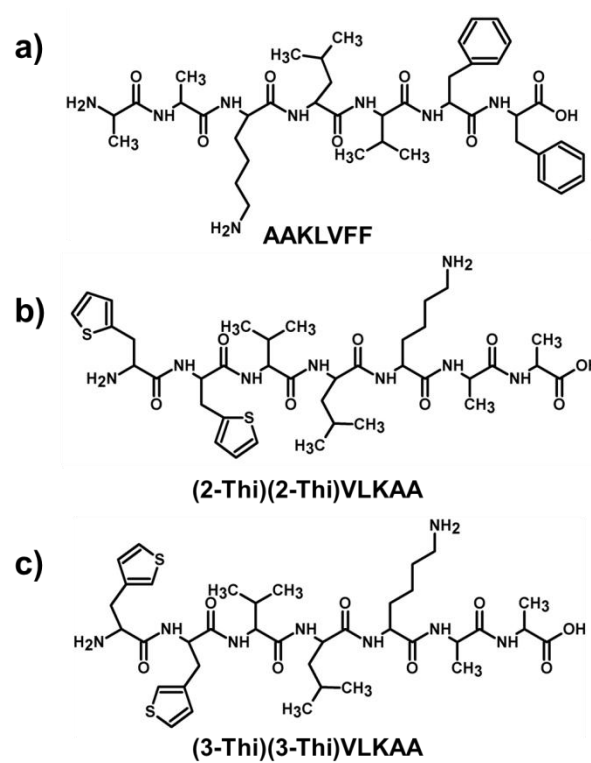
Acknowledgments

Figure 1. Schematic molecular structure of **a)** AAKLVFF, **b)** (2-Thi)(2-Thi)VLKAA, and **c)** (3-Thi)(3-Thi)VLKAA.
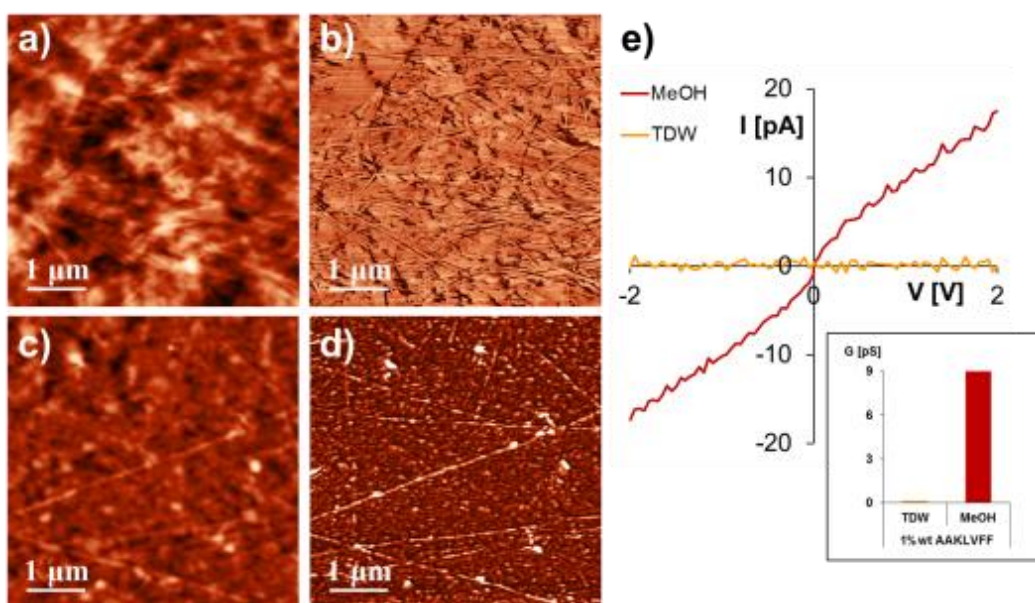
Figure 2. a-b) AFM height and phase images of 1 wt% AAKLVFF assembled in MeOH, respectively (z scale 234 nm and 65°, respectively). **c-d)** AFM height and phase images of 1 wt% AAKLVFF assembled in TDW, respectively (z scale 154 nm and 11°, respectively). **e)** I-V curves and **c**onductance values (inset) of 1 wt% AAKLVFF assembled in either MeOH or TDW. Samples were prepared by drop-drying 5 μl droplets of the solution. Current measurements were obtained under pressure of 10^{-3} mbar.
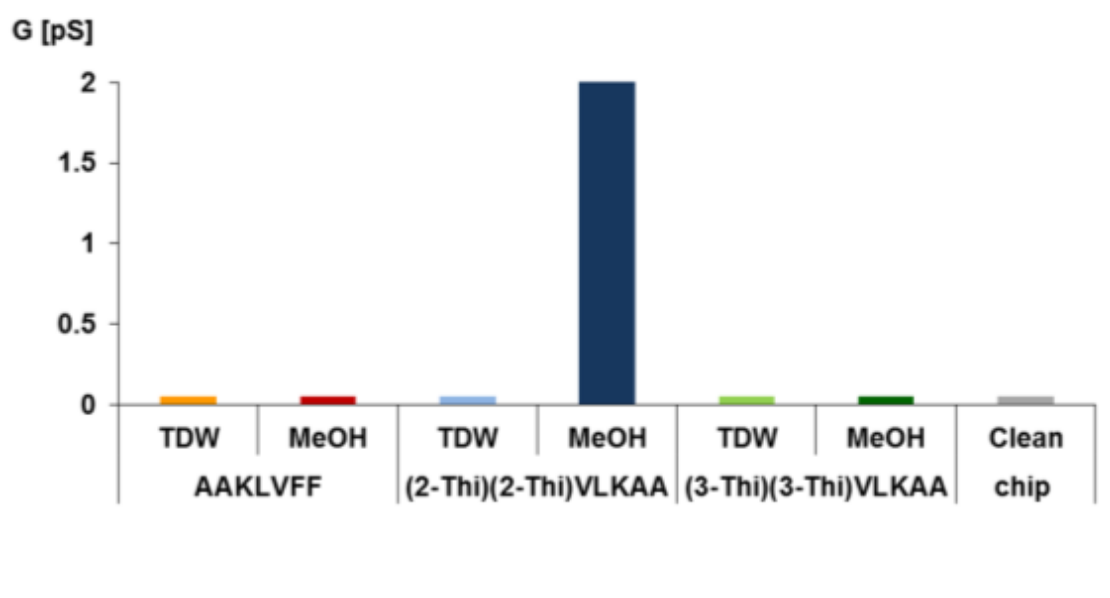
Figure 3. Calculated conductance values of the three different peptides assembled in either TDW or MeOH (0.03 wt% peptide concentration) and of a clean chip, acquired under pressure of 10^{-3} mbar. The error in the conductance values is in the order of 4%.
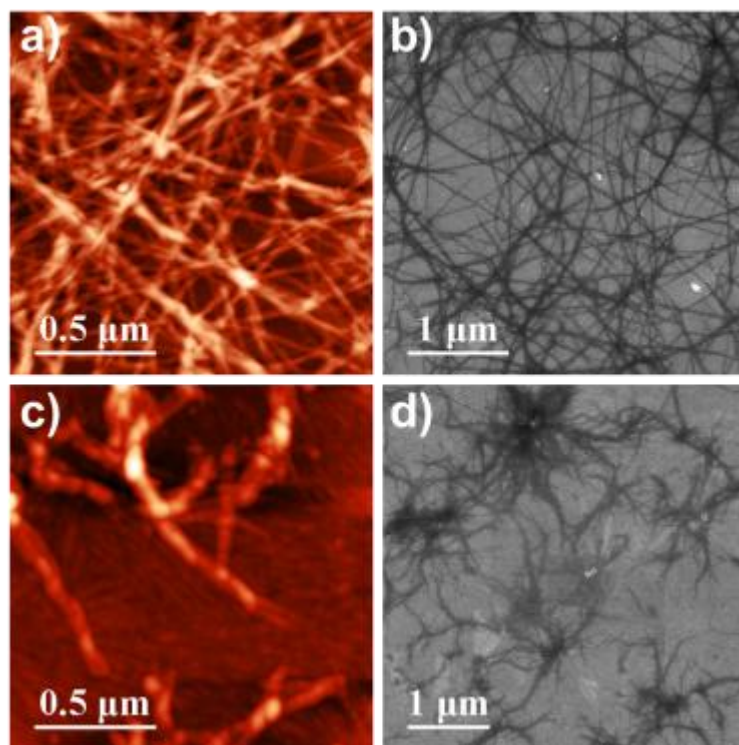
Figure 4. a-b) AFM height (z scale 82 nm) and SEM images, respectively, of 0.03 wt% (2-Thi)(2-Thi)VLKAA assembled in MeOH. **c-d)** AFM height (z scale 24 nm) and SEM images, respectively, of 0.03 wt% (2-Thi)(2-Thi)VLKAA assembled in TDW.
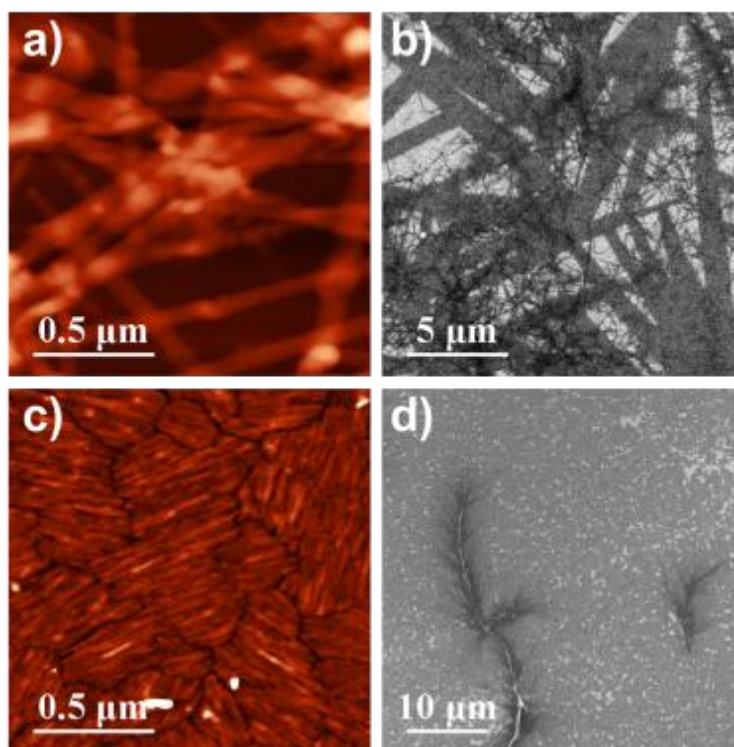
Figure 5. a-b) AFM height (z scale 170 nm) and SEM images, respectively, of 0.03 wt% AAKLVFF assembled in MeOH. **c-d)** AFM height (z scale 15 nm) and SEM images, respectively, of 0.03 wt %AAKLVFF assembled in TDW.
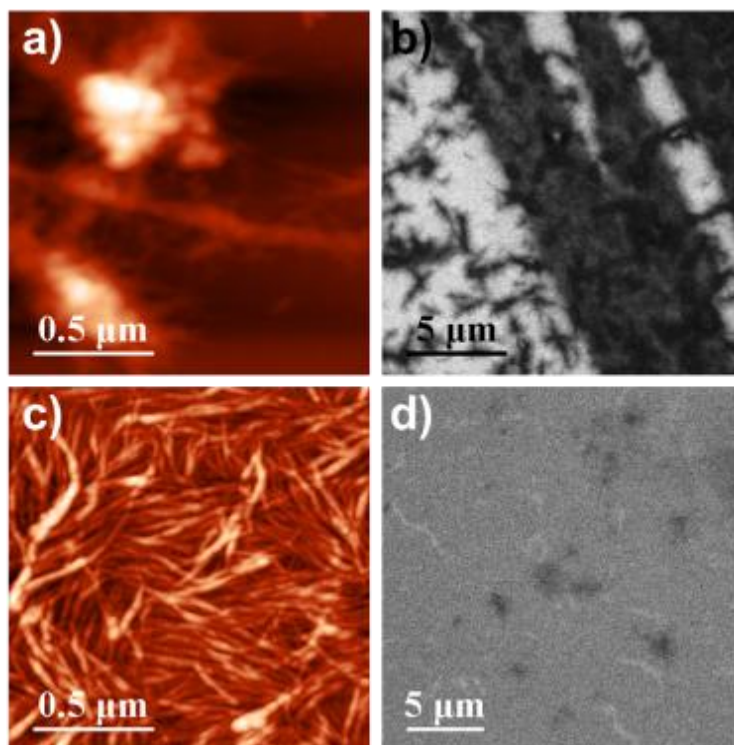
Figure 6. a-b) AFM height (z scale 150 nm) and SEM images, respectively, of 0.03 wt% (3-Thi)(3-Thi)VLKAA assembled in MeOH. **c-d)** AFM height (z scale 35 nm) and SEM images, respectively, of 0.03 wt% (3-Thi)(3-Thi)VLKAA assembled in TDW.
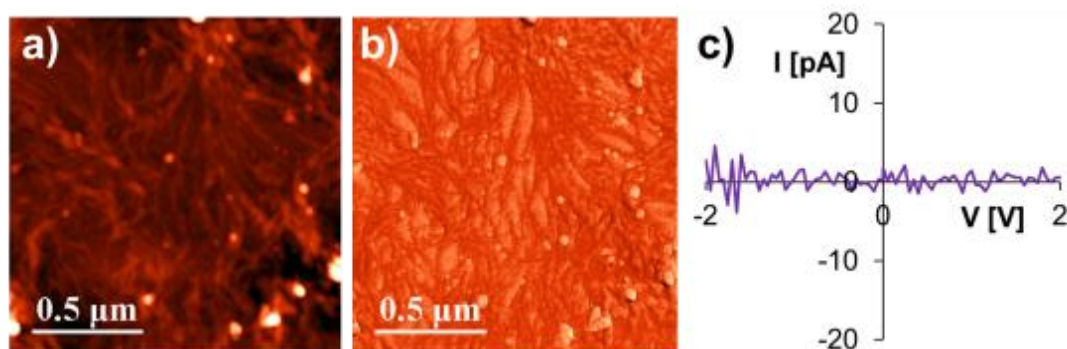
Figure 7. a-b) AFM height and phase images of 15%wt A_6K assembled in TDW, respectively (z scale 25 nm and 5.5°, respectively). **c)** I-V curve and conductance value (inset) of 15%wt A_6K assembled in TDW. Samples were prepared by drop-dry of 2 μl droplets of the solution. Current measurements were obtained under pressure of 10^{-3} mbar.

4   References

1.   B. Caughey and P. T. Lansbury, *Annu. Rev. Neurosci.*, 2003, **26**, 267-298.

2.   R. Nelson, M. R. Sawaya, M. Balbirnie, A. O. Madsen, C. Riekel, R. Grothe and D. Eisenberg, *Nature*, 2005, **435**, 773-778.

3.   V. Castelletto, I. W. Hamley, P. J. F. Harris, U. Olsson and N. Spencer, *J. Phys. Chem. B*, 2009, **113**, 9978-9987.

4.   I. Cherny and E. Gazit, *Angew. Chem., Int. Ed.*, 2008, **47**, 4062-4069.

5.   V. Castelletto, I. W. Hamley, C. Cenker and U. Olsson, *J. Phys. Chem. B*, 2010, **114**, 8002-8008.

6.   V. Castelletto, I. W. Hamley, C. Cenker, U. Olsson, J. Adamcik, R. Mezzenga, J. F. Miravet, B. Escuder and F. Rodriguez-Llansola, *J. Phys. Chem. B*, 2011, **115**, 2107-2116.

7.   P. Kumaraswamy, R. Lakshmanan, S. Sethuraman and U. M. Krishnan, *Soft Matter*, 2011, **7**, 2744-2754.

8.   I. W. Hamley, G. D. Brown, V. Castelletto, G. Cheng, M. Venanzi, M. Caruso, E. Placidi, C. Aleman, G. Revilla-Lopez and D. Zanuy, *J. Phys. Chem. B*, 2010, **114**, 10674-10683.

9.   M. Reches and E. Gazit, *Science*, 2003, **300**, 625-627.

10.   M. J. Krysmann, V. Castelletto, J. E. McKendrick, L. A. Clifton, I. W. Hamley, P. J. F. Harris and S. A. King, *Langmuir*, 2008, **24**, 8158-8162.

11.   V. Castelletto, I. W. Hamley and P. J. F. Harris, *Biophys. Chem.*, 2008, **138**, 29-35.

12.   A. Noy, A. B. Artyukhin and N. Misra, *Mater. Today*, 2009, **12**, 22-31.

13.   A. Noy, *Adv. Mater.*, 2011, **23**, 807-820.

14.   R. de la Rica and H. Matsui, *Chem. Soc. Rev.*, 2010, **39**, 3499-3509.

15.   J. Shklovsky, P. Beker, N. Amdursky, E. Gazit and G. Rosenman, *Mat. Sci. Eng. B-Solid*, 2010, **169**, 62-66.

16.   S. G. Zhang, *Nat. Biotechnol.*, 2003, **21**, 1171-1178.

17.   X. Y. Gao and H. Matsui, *Adv. Mater.*, 2005, **17**, 2037-2050.

18.   R. J. Brea, C. Reiriz and J. R. Granja, *Chem. Soc. Rev.*, 2010, **39**, 1448-1456.

19.   N. Kol, L. Adler-Abramovich, D. Barlam, R. Z. Shneck, E. Gazit and I. Rousso, *Nano Lett.*, 2005, **5**, 1343-1346.

20.   S. Scanlon and A. Aggeli, *Nano Today*, 2008, **3**, 22-30.

21.   L. Adler-Abramovich, M. Reches, V. L. Sedman, S. Allen, S. J. B. Tendler and E. Gazit, *Langmuir*, 2006, **22**, 1313-1320.

22.   L. Adler-Abramovich, D. Aronov, P. Beker, M. Yevnin, S. Stempler, L. Buzhansky, G. Rosenman and E. Gazit, *Nat. Nanotechnol.*, 2009, **4**, 849-854.

23.   N. Amdursky, I. Koren, E. Gazit and G. Rosenman, *J. Nanosci. Nanotechnol.*, 2011, **11**, 9282-9286.

24.   J. S. Lee, I. Yoon, J. Kim, H. Ihee, B. Kim and C. B. Park, *Angew. Chem., Int. Ed.*, 2011, **50**, 1164-1167.

25.   N. Amdursky, A. Handelman and G. Rosenman, *Appl. Phys. Lett.*, 2012, **100**, 103701.

26.   A. Kholkin, N. Amdursky, I. Bdikin, E. Gazit and G. Rosenman, *Acs Nano*, 2010, **4**, 610-614.

27.   J. H. Kim, M. Lee, J. S. Lee and C. B. Park, *Angew. Chem., Int. Ed.*, 2012, **51**, 517-520.

28.   J. H. Kim, J. Ryu and C. B. Park, *Small*, 2011, **7**, 718-722.

29.   R. de la Rica, E. Mendoza, L. M. Lechuga and H. Matsui, *Angew. Chem., Int. Ed.*, 2008, **47**, 9752-9755.

30.   B. J. Pepe-Mooney and R. Fairman, *Curr. Opin. Struct. Biol.*, 2009, **19**, 483-494.

31.   L. L. del Mercato, P. P. Pompa, G. Maruccio, A. Della Torre, S. Sabella, A. M. Tamburro, R. Cingolani and R. Rinaldi, *Proc. Natl. Acad. Sci. U. S. A.*, 2007, **104**, 18019-18024.

32.   J. Castillo, S. Tanzi, M. Dimaki and W. Svendsen, *Electrophoresis*, 2008, **29**, 5026-5032.

33.   H. Xu, A. K. Das, M. Horie, M. S. Shaik, A. M. Smith, Y. Luo, X. Lu, R. Collins, S. Y. Liem, A. Song, P. L. A. Popelier, M. L. Turner, P. Xiao, I. A. Kinloch and R. V. Ulijn, *Nanoscale*, 2010, **2**, 960-966.

34.   W. S. Horne, N. Ashkenasy and M. R. Ghadiri, *Chem.- Eur. J.*, 2005, **11**, 1137-1144.

35.   N. Ashkenasy, W. S. Horne and M. R. Ghadiri, *Small*, 2006, **2**, 99-102.

36.   M. Cordes, O. Jacques, A. Koettgen, C. Jasper, H. Boudebous and B. Giese, *Adv. Synth. Catal.*, 2008, **350**, 1053-1062.

37. F. Rodriguez-Ropero, D. Zanuy, X. Assfeld and C. Aleman, *Biomacromolecules*, 2009, **10**, 2338-2343.

38. M. Reches and E. Gazit, *Nat. Nanotechnol.*, 2006, **1**, 195-200.

39. J. S. Lee, J. Ryu and C. B. Park, *Soft Matter*, 2009, **5**, 2717-2720.

40. P. Beker, I. Koren, N. Amdursky, E. Gazit and G. Rosenman, *J. Mater. Sci.*, 2010, **45**, 6374-6378.

41. M. Mizrahi, A. Zakrassov, J. Lerner-Yardeni and N. Ashkenasy, *Nanoscale*, 2012, **4**, 518-524.

42. I. Ron, L. Sepunaru, S. Itzhakov, T. Belenkova, N. Friedman, I. Pecht, M. Sheves and D. Cahen, *J. Am. Chem. Soc.*, 2010, **132**, 4131-4140.

43. L. Sepunaru, I. Pecht, M. Sheves and D. Cahen, *J. Am. Chem. Soc.*, 2011, **133**, 2421-2423.

44. R. Langen, I. J. Chang, J. P. Germanas, J. H. Richards, J. R. Winkler and H. B. Gray, *Science*, 1995, **268**, 1733-1735.

45. B. Q. Q. Xu, X. L. L. Li, X. Y. Y. Xiao, H. Sakaguchi and N. J. J. Tao, *Nano Lett.*, 2005, **5**, 1491-1495.

46. J. Liao, J. S. Agustsson, S. Wu, C. Schoenenberger, M. Calame, Y. Leroux, M. Mayor, O. Jeannin, Y.-F. Ran, S.-X. Liu and S. Decurtins, *Nano Lett.*, 2010, **10**, 759-764.

47. B. D. Wall, S. R. Diegelmann, S. Zhang, T. J. Dawidczyk, W. L. Wilson, H. E. Katz, H.-Q. Mao and J. D. Tovar, *Adv. Mater.*, 2011, **23**, 5009-5014.

48. S. Kothakota, T. L. Mason, D. A. Tirrell and M. J. Fournier, *J. Am. Chem. Soc.*, 1995, **117**, 536-537.

49. S. Bucak, C. Cenker, I. Nasir, U. Olsson and M. Zackrisson, *Langmuir*, 2009, **25**, 4262-4265.

50. V. Castelletto, D. R. Nutt, I. W. Hamley, S. Bucak, C. Cenker and U. Olsson, *Chem. Commun.*, 2010, **46**, 6270-6272.
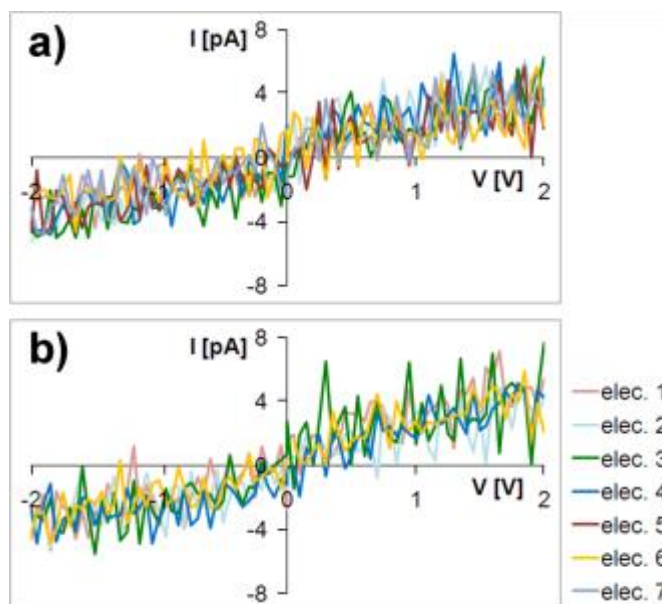
5   Supplementary information

Figure S1. I-V measurements of 0.03%wt (2-Thi)(2-Thi)VLKAA assembled in MeOH carried out on **a)** chip 1 and **b)** chip 2 in vacuum of 10^{-3} mbar.
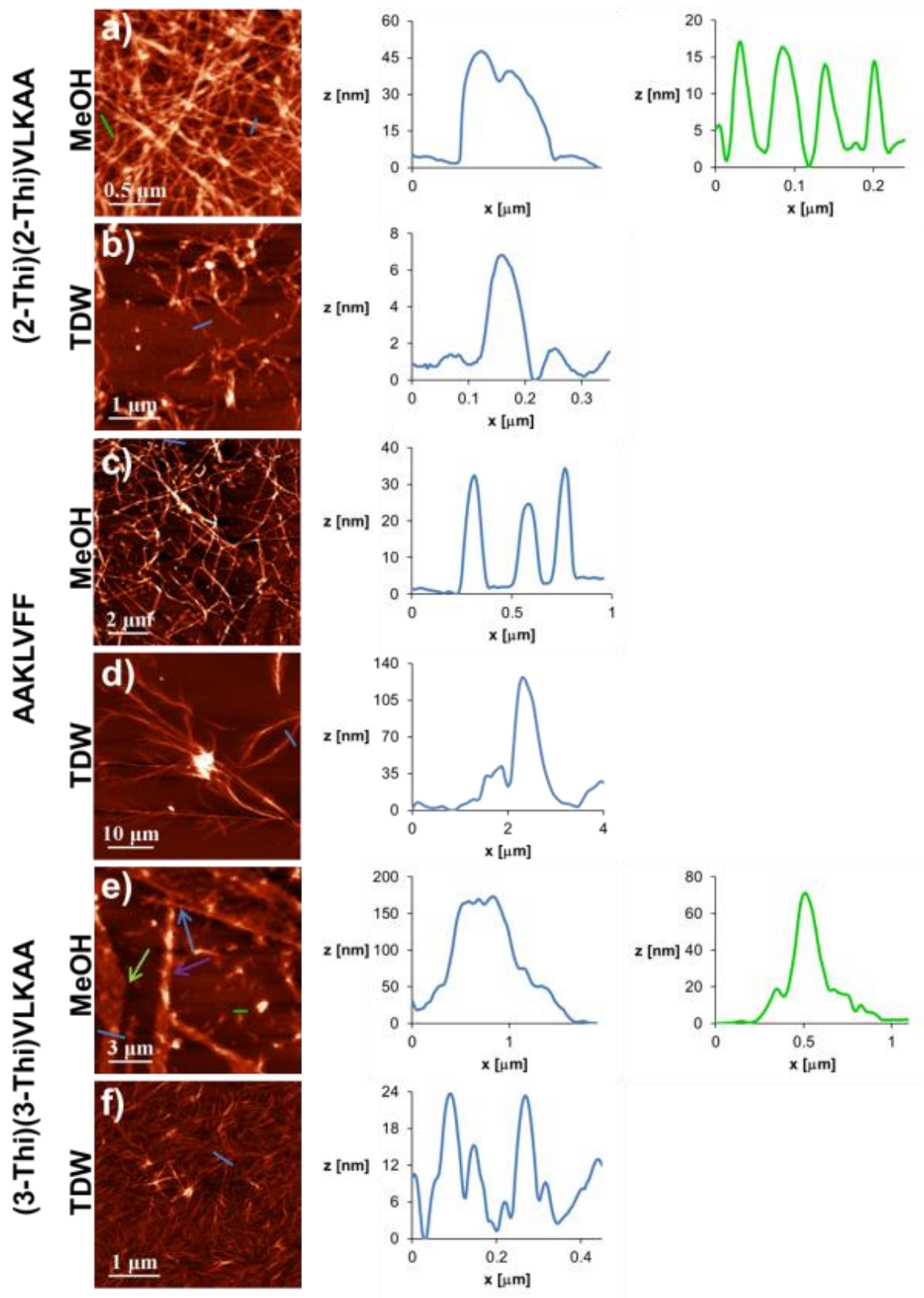
Figure S2. a) AFM height (z scale 88 nm) and the corresponding cross-sections across the blue and green lines of 0.03%wt (2-Thi)(2-Thi)VLKAA assembled in MeOH, showing fibers with diameter of ~45 nm and ~13 nm, respectively. **b)** AFM height (z scale 33 nm) and the corresponding cross-section across the blue line of 0.03%wt (2-Thi)(2-Thi)VLKAA assembled in TDW, showing bundled fibers with diameter of ~6 nm. **c)** AFM height (z scale 86 nm) and the corresponding cross-section across the blue line of 0.03%wt AAKLVFF assembled in MeOH, showing fibers with diameter of ~30 nm. **d)** AFM height (z scale 330 nm) and the corresponding cross-section across the blue line of 0.03%wt AAKLVFF assembled in TDW, showing branched fibers with diameter of ~120 nm. **e)** AFM height (z scale 460 nm) and the corresponding cross-sections across the blue and green lines of 0.03%wt (3-Thi)(3-Thi)VLKAA assembled in MeOH, showing wide tapes with height of ~150 nm (blue line), either folded or twisted (green and purple arrows, respectively), and bundled fibers (blue arrow) with diameter of ~70 nm (green line). **f)** AFM height (z scale 58 nm) and the corresponding cross-section across the blue line of 0.03%wt (3-Thi)(3-Thi)VLKAA assembled in TDW, showing twisted fibers with diameter of ~23 nm.